PAPER

Check for updates

Characterizing the stability of ultra-thin metal oxide catalyst films in non-thermal plasma CO_2 reduction reactions†

Samuel K. Conlin, [ID] [a] Joseph Joel Muhanga,[b] David N. Parette [ID] [a] and Robert H. Coridan [ID] ★[ab]

The use of metal oxide catalysts to enhance plasma CO_2 reduction has seen significant recent development towards processes to reduce greenhouse gas emissions and produce renewable chemical feedstocks. While plasma reactors are effective at producing the intended chemical transformations, the conditions can result in catalyst degradation. Atomic layer deposition (ALD) can be used to synthesize complex, hierarchically structured metal oxide plasma catalysts that, while active for plasma CO_2 reduction, are potentially vulnerable to degradation due to their high surface area and nanoscopic thickness. In this work, we characterized the effects of extended non-thermal, glow discharge plasma exposure on ALD synthesized, ultra-thin film (<30 nm) TiO_2 and ZnO catalysts. We used X-ray diffraction, reflectivity, and spectroscopy to compare films exposed to a CO_2 plasma to ones exposed to an Ar plasma and to ones annealed in air. We found that the CO_2 plasma exposure generated some surface reduction in TiO_2 and increased surface roughening by a small amount, but did not initiate any phase changes or crystallite growth. The results suggest that ALD-deposited metal oxide films are robust to low pressure CO_2 plasma exposure and are suitable as catalysts or catalyst supports in extended reactions.

Introduction

The goal of limiting global warming to a 2 °C increase over pre-industrial temperatures will require a substantial global reduction in the release of greenhouse gases, primarily CO_2.[1] The development of carbon dioxide removal (CDR) technologies, also referred to as negative emissions technologies (NET), will be necessary to achieve a carbon-negative economy.[1–3] One route to this is to use electrical power to drive chemical reactions in a gas-phase plasma reactor. High local electric field densities can result in electrons with high average kinetic energies. These electrons can interact with gas phase species to produce radicals. This can result in endergonic, fuel forming reactions. By using a thermal or non-thermal plasma system, captured CO_2 can be split into CO and $\frac{1}{2}O_2$, for example. If the plasma is driven by renewable electricity, the produced CO can then be used as a carbon-neutral industrial feedstock,[4–7] or further reduced in the plasma to C and sequestered as a carbon-negative technology.[8–10] Thermal and non-thermal glow discharge plasmas have been shown to have single pass CO_2

conversion yields of upwards of 30% and energy efficiencies exceeding 58%, with overall conversion and energy efficiency depending heavily on the reactor and plasma conditions.[11–13]

In plasma CO_2 reactors, heterogeneous catalysts are often included in the discharge region to increase overall CO_2 conversion yield and energy efficiency.[4,5,7,14] One important class of heterogeneous catalysts are earth-abundant metal oxides, commonly in the form of pellets, spheres, or a packed bed.[15–19] These catalysts generally improve overall performance by providing active sites for CO_2 reduction, typically in the form of oxygen vacancies (V_o). These oxygen vacancies are formed by surface–plasma interactions such as direct ion bombardment and reaction of the surface with atomic O produced in the gas phase. The reduction of CO_2 to CO occurs at the under-coordinated metal sites associated with the oxygen vacancies, and the reaction replaces the missing lattice O.[20,21] The catalysts also act as a dielectric, enhancing the electric field near the interface and producing local regions of high electric field and electron density, especially near surface asperities.[22,23] To be useful in plasma reactors, catalyst surfaces need to be robust to the high temperatures, fields, and ion bombardment generated in the plasma–surface interface. While heterogeneous plasma catalysts with large scale features provide stable CO_2 reduction and CO_2 hydrogenation, little is known about degradation and mass loss at the plasma–catalyst interface. Analysis of degradation is particularly important for catalysts engineered with nanoscale architectures to impart specific function or generate

aDepartment of Chemistry and Biochemistry, University of Arkansas, Fayetteville, AR, 72701, USA. E-mail: rcoridan@uark.edu

bMaterials Science and Engineering Program, University of Arkansas, Fayetteville, AR, 72701, USA

high active surface areas. For example, ultra-thin catalyst layers on high surface area supports can be synthesized using atomic layer deposition (ALD) to significantly increase catalytic activity and yield. These layers were shown to have significant catalytic activity in a dielectric breakdown (DBD) plasma CO_2 reactor, though their longevity under extended CO_2 plasma exposure was not investigated.[24] The robustness of these layered materials is necessary for prolonged activity. The deposition of carbon (coking) across the surface of the catalyst can block active catalytic sites. Coking has been shown to occur during both CO_2 and CO reduction at high input powers over long time periods on Fe-based catalysts. It is far more prevalent during CO reduction, however.[9] Another failure mode is the removal of the catalyst layer or its substrate by etching.[25,26] Plasma etching of thin films has been used extensively throughout the semiconductor industry, primarily as reactive ion etching (RIE) for material processing.[26–28] In plasma CO_2 reduction, the products of interest in the gas phase are the CO and atomic O produced from direct CO_2 splitting. The produced CO contributes to carbon deposition while the O contributes to etching of both deposited carbon and the film.[29] The relative ratio of CO and O in CO_2 or CO plasmas is dependent on input power and the duration of the plasma reaction.[29,30] This suggests that under some conditions, the stability of catalysts that are only a few hundred atoms thick could be compromised due to etching. Sputtering, or etching *via* collision of high energy ions with the film, is another potential degradation route and is less dependent on the chemistry of the plasma than reactive etching.[31–34] Given the harshness of the plasma reaction process, the long-term stability of ultra-thin film metal oxide catalysts requires further investigation.[35–38]

Here, we characterize the stability of ALD-derived, ultra-thin film (<30 nm) TiO_2 and ZnO catalyst layers in a low-pressure CO_2 and Ar glow discharge non-thermal plasma reactor. TiO_2 has been used extensively as a component of catalysts for plasma CO_2 reduction and can be etched by both RIE and ion bombardment.[16,39–43] ZnO has been primarily used as a support for catalysts in plasma CO_2 methanation due to the strong metal–support interaction exhibited.[38,44–46] ZnO is also capable of being etched by ion-bombardment and RIE.[43,47–49] We examined the effects of extended plasma exposure on the ALD film structure to understand how the surface and morphology of films change. Plasma exposure can alter the chemistry of the surface *via* reduction, particularly in the case of TiO_2. However, we observed no significant crystallization and only a small degree of surface roughening for either of these materials. No mass losses were observed for the as-deposited TiO_2 and ZnO films even after several hours of exposure to a 25 W input power CO_2 glow discharge. This suggests that nanoscopic films deposited by ALD can be used as robust plasma catalysts in systems designed to operate for extended time periods.

Materials and methods

Acetone (HPLC, BDH), methanol (HPLC, BHD), isopropanol (HPLC, Macron), and water (HPLC, BDH) were used as received. Si wafers (n-type, As-doped, 2 SEMI polished, <0.5 nm

roughness, 0.001–0.004 Ω cm, $\langle 100 \rangle$ orientation; Purewafer) were cleaved to the noted size and used as substrates for ALD film deposition as received. Pyrex glass tubes (Corning) were cut to 85 cm in length and used as the reactor chamber. Glass microscope slides (United Scientific) were cut to the noted size and used to hold the ALD-coated substrates in the plasma chamber. CO_2 (99.999%, Airgas) and Ar (99.999%, Airgas) were used as the reactive atmosphere as received.

ALD of metal oxide films onto Si substrates

Sections of the as-received Si wafers were scribed and cleaved to 1×4 cm^2 in size and cleaned using a successive solvent wash of acetone, isopropanol, methanol, and water. The samples were then dried under a stream of dry N_2 and placed in a UV-Ozone cleaner (Novascan PSD) for 30 minutes. Once exposed, the substrates were then used as prepared for ALD of metal oxide films. The ALD films were grown using a commercial ALD reactor (GEMstar XT-D; Arradiance, Inc.) by sequential exposure of an organometallic precursor and water (HPLC grade; BDH) as an oxygen source. The precursors were contained in a metal-gasket sealed bellows and pulsed into the reaction chamber under continuous dry N_2 flow at 20 sccm at reduced pressure. The precursor tetrakis(dimethylamido)titanium (abbreviated TDMAT, 99%; Strem) was used for depositing TiO_2 and was heated to 75 °C to increase its vapor pressure. The precursor diethylzinc (DEZ, 95%; Strem) was used for depositing ZnO. The specifics of the ALD cycle for each precursor are provided in the ESI.†

Each sample consisted of an approximately 20 nm thick layer of material deposited onto a Si wafer substrate with a native SiO_2 layer. The chosen cycle numbers were calculated from rough growth rates calculated from scanning electron microscopy cross-sectional imaging.[50] This consisted of 404 ALD cycles of TDMAT/H_2O to prepare TiO_2, and 123 cycles of DEZ/H_2O for each sample. These thicknesses were chosen to ensure that the metal oxide layer was sufficiently thick that changes in film thickness or roughness could be evaluated by determining the amount of metal oxide remaining, even in the case of excessive etching by CO_2 plasma. After the ALD reaction, the samples were removed and used as-prepared in the low-pressure glow discharge reactor. Each sample of ALD TiO_2 and ALD ZnO measured here were synthesized under the same respective deposition conditions. This ensured that samples of as prepared films were identical in terms of film thickness, roughness and density as to be expected from the ALD process.

Thermal annealing of ALD metal oxide films

For comparison to the transformations occurring in the CO_2 plasma reactor, samples of TiO_2 and ZnO were prepared identically by ALD, then annealed in air at 500 °C for three hours (ramp 3 °C min^{-1} from room temperature). Once cooled to room temperature, these samples were removed from the reactor and stored in air for at least 24 hours before being examined.
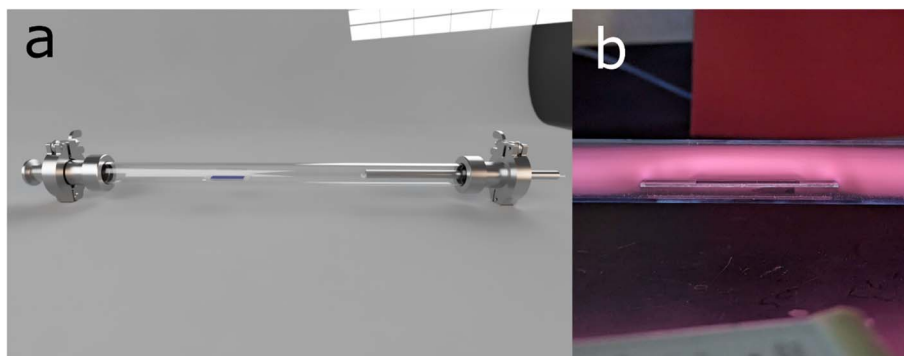
Fig. 1 (a) A rendered schematic of the reactor consisting of the modified electrodes and vacuum ports, Pyrex glass exterior tube, and the sample stage and sample in the discharge region. (b) An image of the sample region during operation, shielding omitted for clarity.

Low pressure plasma exposure of ALD metal oxide films

A custom reactor was constructed to expose the TiO_2 and ZnO films to low pressure CO_2 plasma (Fig. 1). The reactor consisted of a Pyrex glass tube (50 cm long, 25 mm OD, 21.65 mm ID) fitted with vacuum flanges modified to accommodate gas and electrical passthroughs. The reactor was evacuated to 1000 mTorr (Trivac E2) while under continuous CO_2 or Ar flow from a pressure calibrated mass flow controller (SmartTrak Sierra-50). An AC transformer (20 kV, 19 kHz, Allanson SS1235OX) was used to generate the plasma in the discharge region (38 mm wide) located within the tube between the inlet vacuum flange and the outlet vacuum flange. The power provided to the input side of the transformer, denoted input power, was controlled using a variable autotransformer. The power output of the autotransformer was monitored by an inline power meter and was maintained at a single set point throughout the experiment. The sample was placed on the microscope slide glass sample stage in the middle of the discharge region, which elevated the sample 7 mm into the column to ensure homogenous plasma exposure across the entire sample. The reactor was not cooled during testing. The exterior temperature of the reactor was monitored using a thermal camera (Shot-Pro, SEEK Thermal) during the plasma exposure. The exterior temperature tube maintained a relatively low temperature (<72 °C) during each experiment (Fig. S1†).

The as-prepared samples were placed onto the sample stage in the middle of the discharge region. The reactor was then evacuated by a vacuum pump while being purged with the input gas of interest at 500 sccm for 30 min. Once purged, the flow rate of gas was reduced to 50 sccm and the system was left to stabilize for another 20 min. The plasma was initiated after the pressure stabilized and the input power was set to 25 W. The sample was exposed to this continuous plasma for three hours, after which the reactor was turned off and allowed to cool to room temperature under continuous gas flow at reduced pressure. The reactor was then restored to atmospheric pressure under the same gas flow. The sample was then removed and stored in air. While the details of the glow discharge plasma in the reactor were not characterized directly, each sample was exposed to a plasma generated using the same apparatus, under identical reactor pressure, mass flow controller, and AC transformer settings.

ALD metal oxide film characterization

Film thickness, surface roughness, and density were derived from X-ray reflectance (XRR) measurements taken using a PANalytical X'Pert PRO X-ray diffractometer equipped with a MRD Cradle system for sample positioning, utilizing the $K\alpha_1$ line from a Cu rotating anode with a pre-sample monochromator ($\lambda = 1.5406$ Å). To characterize changes in ALD film thickness and roughness due to plasma exposure, model structures were produced using the X'Pert Reflectivity software package. X-ray diffraction measurements (XRD) of the plasma catalysts were taken using a Rigaku Mini-Flex II X-ray diffractometer using the $K\alpha_1$ line from a Cu anode ($\lambda = 1.54$ Å). X-ray photoelectron spectroscopy (XPS) measurements performed on a PHI Versaprobe spectrometer equipped with a monochromatic Al source (incident energy = 1486.6 eV). Measurements were taken with a spot size of 100 μm × 100 μm. XPS data was calibrated to the adventitious C 1s feature (binding energy = 284.8 eV) and analyzed using the CasaXPS software package. Details on the analysis and fitting procedures used here can be found in the ESI.†

Results and discussion

Structural and surface characterization of plasma-exposed ALD-metal oxide films

The bulk structure of the ALD films was analyzed using XRD before and after plasma exposure to determine if long-term plasma exposure caused any chemical changes in the crystal structure that could result in, for example, a volume change. The effects of plasma exposure on as-prepared TiO_2 were compared to those of thermal annealing as-prepared TiO_2 in air. The as-prepared sample was found to be amorphous, lacking any Bragg reflections that would indicate any crystalline phase even outside of the region of interest in Fig. 2. This small range was investigated with an extremely slow scan (rate = $0.02°$ min^{-1}) due to the low intensity of any Bragg reflections that may originate from the roughly 20 nm films investigated here. The observation of amorphous TiO_2 films is consistent
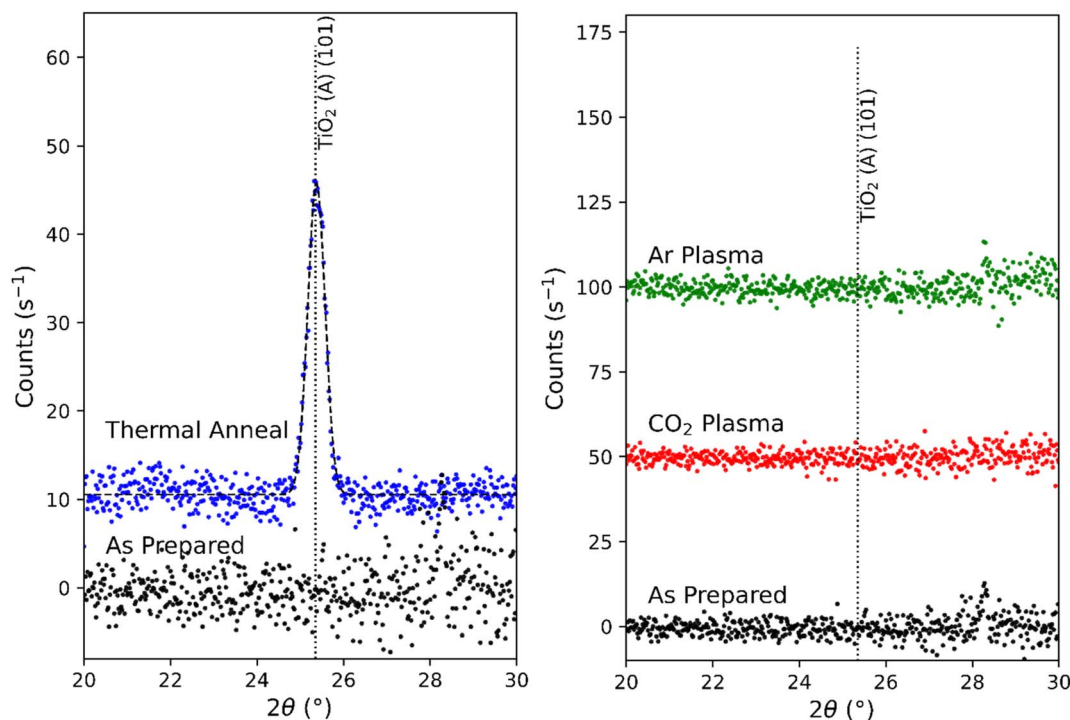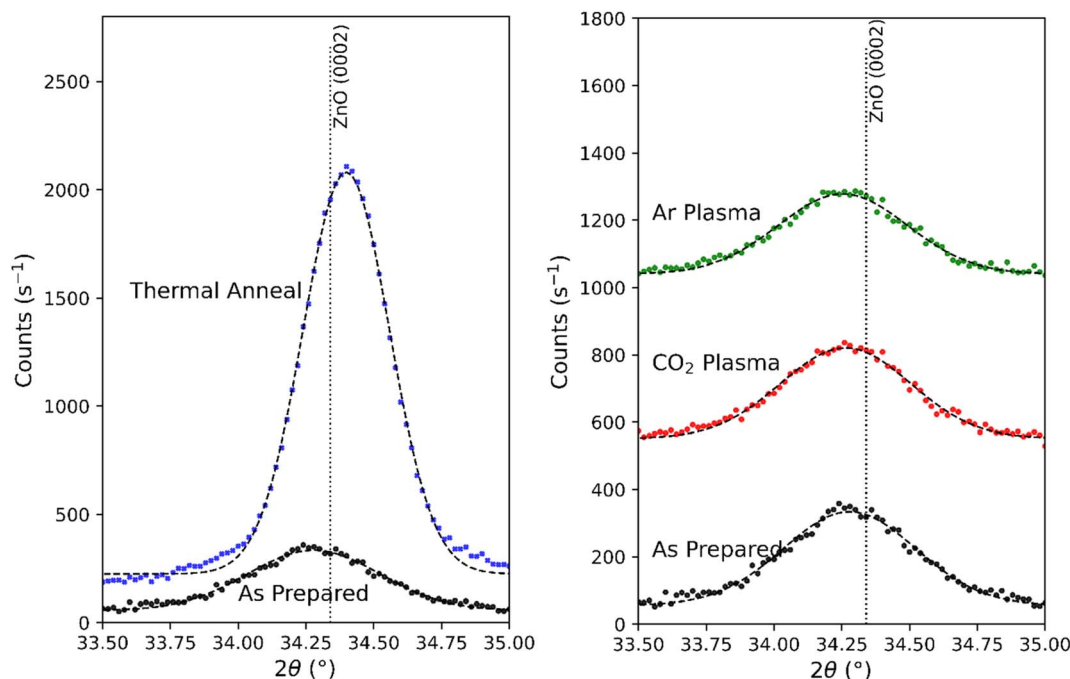
Fig. 2 The X-ray diffraction (XRD) measurements of (left) as-prepared (black), annealed (blue) and (right) as-prepared (black), CO_2 plasma-exposed (red), and Ar plasma-exposed (green) TiO_2. Dots indicate the measured data after subtracting the signal for the empty substrate holder. Dashed lines indicated the Gaussian fit used to determine the crystallite size where applicable. The vertical dotted line indicates the indexing of the most prominent peak ($2\theta = 25.4°$) corresponding to the (101) Bragg reflection of anatase TiO_2.

Fig. 3 XRD measurements of (left) as prepared (black), annealed (blue) and (right) as-prepared (black), CO_2 plasma-exposed (red), and Ar plasma-exposed (green) ZnO. Dots indicate the measured data after subtracting the signal for the empty substrate holder. Dashed lines indicated the Gaussian fit used to determine the crystallite size where applicable. Vertical dotted line indicates the index of the most prominent peak observed at $2\theta = 34.3°$ corresponding to the (0002) Bragg reflection in the standard, room temperature wurtzite phase of ZnO. Offset from indexes were due to small sample positioning variations.

with other reports of films synthesized by thermal ALD under the same conditions.[51,52] A prominent Bragg reflection at $2\theta = 25.4°$ was observed for the TiO_2 film that had only been annealed, indicating that it had crystallized into the anatase phase. No new peaks were observed in the films exposed to either CO_2 or Ar plasma, indicating that they remained amorphous for the duration of the experiment. We analyzed the peak shape on the annealed film to assess the microstructure that had formed. The details of the analysis and calibration of the instrumental broadening can be found in the ESI.† The Debye–Scherrer (DS) crystallite size of the annealed TiO_2 film was found to be 18.7 nm (eqn (S1)†).[53] While we could be certain that the films had crystallized under thermal annealing conditions, the lack of any emergent Bragg scattering in extended XRD measurements implied that the as-prepared TiO_2 films did not undergo any phase change due to the thermal effects of plasma exposure. The film did not undergo any volume changes which could contribute to crack formation which would compromise the integrity of the catalyst layer.[54,55] This is supported by temperature measurements of the reactor during operation, in which the reactor walls adjacent to the sample region did not exceed 70 °C (Fig. S1†).

The structure of ZnO films before and after CO_2 or Ar plasma exposure were also examined by XRD, as shown in Fig. 3. In contrast to the as-prepared TiO_2 films, some crystallinity was observed in the as-prepared ZnO films after the ALD synthesis.[51] The intense peak at $2\theta = 34.3°$ was indexed to the (0002) Bragg reflection of wurtzite ZnO. We used this Bragg reflection to determine the DS crystallite size of the as prepared and post-plasma exposed films. The as-prepared ZnO had an average DS crystallite size of 15.6 nm, which showed a negligible difference after CO2 and Ar plasma exposure (15.7 nm and 15.9 nm after exposure, respectively). In contrast, thermal annealing caused an observed increase in average crystallite size, to 24.61 nm. This again suggests that the thermal and chemical effects associated with the plasma exposure studied here resulted in minimal changes to the bulk crystallinity of the films. It also suggests that any changes in film thickness or roughness over time are likely due to plasma effects rather than bulk crystallization.

XPS is sensitive to the composition and oxidation state of a surface. We used XPS to characterize chemical changes to the surface of the of the as-prepared, plasma-exposed, and annealed samples. The surface composition and oxidation state of the samples were examined after the noted treatment, and samples were left in air for one day prior to XPS characterization. The as-prepared TiO_2 catalyst showed intense features at 458.1 eV and 464.0 eV, which correspond to the Ti $2p_{3/2}$ and Ti $2p_{1/2}$ features respectively (Fig. 4a) and are consistent with standard measurements of TiO_2 (Ti^{4+}).[56] After thermal annealing, these same features corresponding to the Ti $2p_{3/2}$ and Ti $2p_{1/2}$ features were found at 458.1 eV and 464.0 eV respectively (Fig. 4b). In contrast to the as-prepared TiO_2 sample, additional features were observed in the XPS spectra of the CO_2 plasma-exposed sample (Fig. 4c). New features in the Ti $2p_{3/2}$ and Ti $2p_{1/2}$ spectra were observed at 457.3 eV and 462.9 eV, respectively, indicating the formation of reduced Ti^{3+} species at the
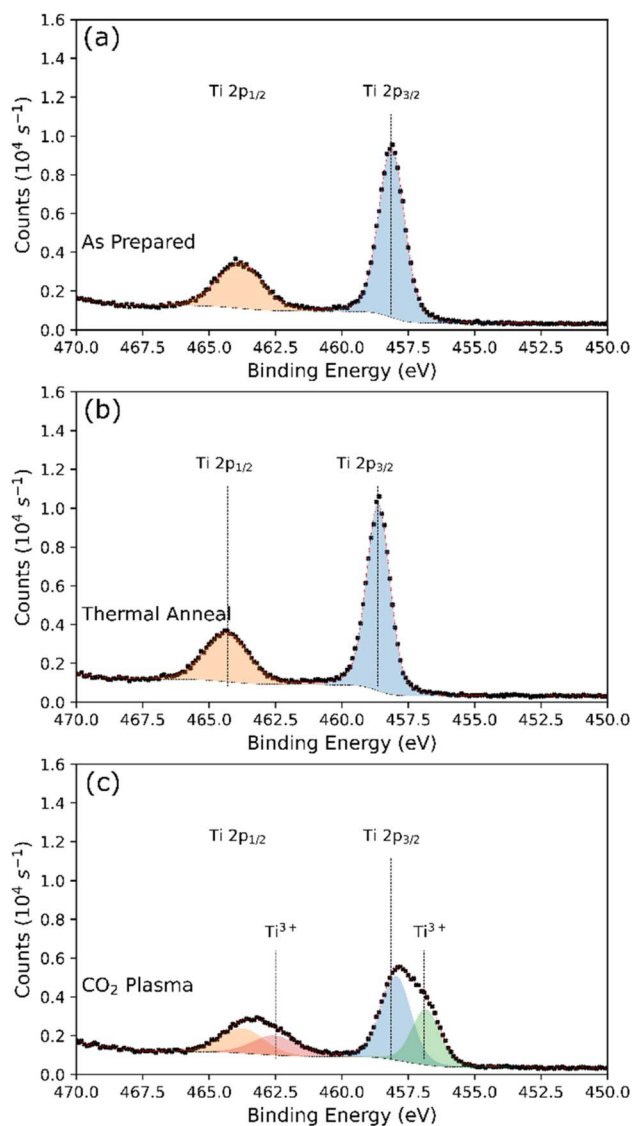

Fig. 4 XPS of the Ti 2p region measured on (a) as prepared, (b) annealed, (c) CO_2 plasma-exposed TiO_2. The red dashed line indicates the sum of fitted features. Dots indicate the measured data, and the dashed line indicates the fitted baseline.

surface.[57] The formation of Ti^{3+} species after plasma exposure has been previously reported. It is considered to indicate the formation of an undercoordinated metal site which serves as an active site for catalytic plasma CO_2 reduction.[20] In air, this may indicate the formation of Ti_2O_3, though no indication of this was observed in XRD measurements.[58] The total integrated intensity of the Ti $2p_{3/2}$ and Ti $2p_{1/2}$ features was roughly conserved between the CO_2 plasma-exposed film and the as-prepared one, which suggests that the surface is not obscured by carbon deposition at 25 W input power.

The as-prepared ZnO sample, Fig. 5a, showed a significant feature at 1023 eV in the Zn $2p_{3/2}$ spectrum, corresponding to ZnO (Zn^{2+}).[59] After thermal annealing, we observed a slight broadening of the Zn $2p_{3/2}$ feature, though the central position of the peak was unchanged (Fig. 5b). This spectrum provides no
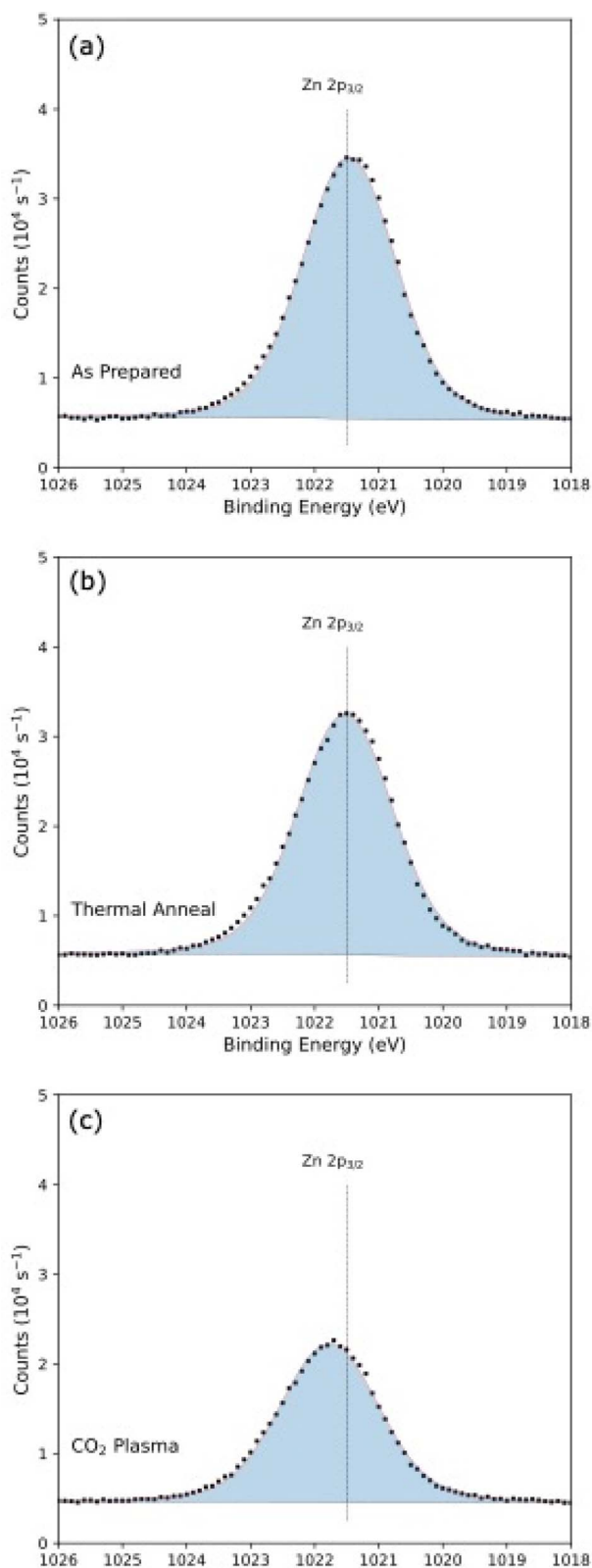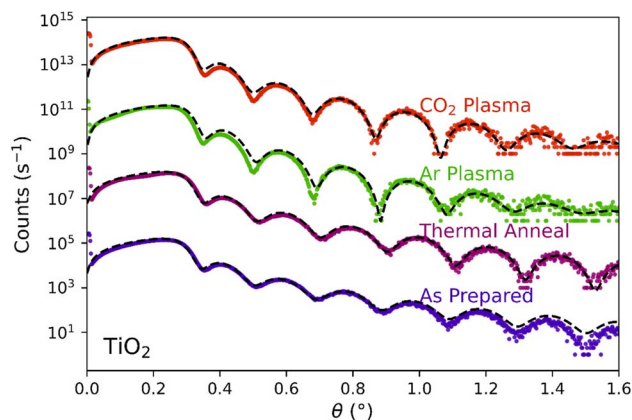
Fig. 5 XPS of the Zn 2p region (a) as-prepared, (b) annealed, (c) CO_2 plasma-exposed ZnO. The red dashed line indicates the sum of fitted features. Dots indicate the measured data, and the dashed line indicates the fitted baseline.

Fig. 6 XRR spectra (from bottom to top) of as deposited (blue), annealed (magenta), Ar plasma-exposed (green), and CO_2 plasma-exposed (red) ALD-deposited TiO_2. The dashed line with each spectrum indicates the XRR spectra of the corresponding model structure. Each spectrum was offset by roughly 10^3 on the logarithmic scale in the plot to provide visual separation. The intensity for each measurement was consistent for each sample.

indication of reduced Zn species in the ZnO film, which is supported by examination of the Zn LMM Auger region. Zn LMM Auger spectroscopy is more sensitive to Zn reduction than Zn 2p XPS (Fig. S2†).[60] While the reduction of ZnO to Zn has been observed at high temperatures both in air and in the presence of carbon, we did not find evidence of reduced Zn species in the annealed sample or in the CO_2 plasma-exposed samples (Fig. 5c).[61,62] Measurements of the of the Zn LMM Auger region also found the plasma-exposed samples were indistinguishable from the other samples (Fig. S2†). If reduced Zn^{1+} or Zn^0 atoms are produced during the plasma exposure, observing them likely requires more sophisticated, air-free transfer of the sample to the analysis chamber. We did not observe intensity from the substrate in the Si 2s XPS spectra that would indicate the thinning of the ALD layers in any of the samples measured here. The presence of the Zn 2p and Ti 2p XPS signals in the plasma-exposed samples, as well as the intense Bragg peak in the XRD of the plasma exposed ZnO, suggests that at these scales, both ultra-thin film layers are robust to extended CO_2 plasma exposure over the duration of these experiments.

A more sensitive probe was necessary to characterize nanoscale morphological changes in each film. We used XRR to characterize the film thickness, average surface roughness and density of the ALD films to sub-nanometer resolution. Fig. 6 shows the resulting XRR measurements for the TiO_2 films, along with model structures overlaying the relevant data. The parameters for the corresponding XRR models for average film thickness, roughness, and density are found in Table 1. After exposure to CO_2 plasma, the roughness of the TiO_2 film increased from 0.53 nm to 1.03 nm. This increase in roughness was associated with a slight increase in film thickness to 21.09 nm to 21.53 nm and decrease in film density. A similar increase in film roughness and corresponding small increase in average thickness was found for the sample exposed to the Ar plasma. The annealed sample exhibited a lower average film

Table 1 The model structures of corresponding to XRR spectrum for each sample

Sample		Thickness (nm)	Roughness (nm)	Density (g cm^{-3})
TiO$_2$-	As prepared	21.09	0.53	3.83
	Thermal anneal	20.64	0.60	3.85
	Ar plasma	21.20	1.17	4.00
	CO$_2$ plasma	21.53	1.03	3.72
ZnO-	As prepared	27.50	1.30	5.61
	Thermal anneal	27.67	1.88	5.75
	Ar plasma	27.90	2.39	5.48
	CO$_2$ plasma	28.87	2.28	5.69

roughness, 0.60 nm, than the plasma-exposed samples. This corresponded to a small decrease in film thickness and increase in film density, which is consistent with the observed crystallization of the film and a slight change in volume.

The XRR measurements and corresponding model structures for the ZnO films are shown in Fig. 7. In the case of CO$_2$ and Ar plasma exposure, the film average roughness increased from 1.30 nm to 2.28 nm and 2.39 nm respectively. Both films also exhibited a small (<1 nm) increase in film thickness which is consistent with the observed increase in film roughness. Overall, the films that were exposed to the plasma indicated no loss of material, suggesting that the as-prepared ALD films were not significantly etched by intermediates produced from gas–plasma interactions. The plasma-exposed films also exhibited an increase in average surface roughness. This is possibly caused by energetic ion bombardment at the plasma–film interface, which has been shown to be capable of roughening film surfaces on a nanoscale and producing surface asperities,
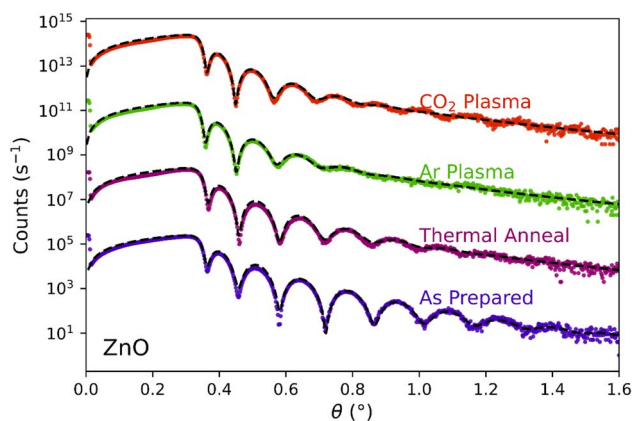
and can redistribute etched material across the film.[42,63,64] The roughening effects were also independent of the chemical nature of the plasma (Ar *versus* CO$_2$). This also supports the conclusion that the material is not being etched, which would likely result in a smoothing of the surface rather than in increase in roughness.[43,65] This was not the case in these experiments.

Conclusions

We examined the crystal structure and morphology of ALD-synthesized ultra-thin TiO$_2$ and ZnO films before and after extended exposure to a CO$_2$ glow discharge plasma. The use of ALD is significant as it allows precise control over the thickness of the deposited catalyst and can produce surfaces of sub-nanometer average roughness over large surface areas. This provided an understanding of how the surface profile and film thickness of metal oxide plasma catalysts can be expected to change because of exposure to the ionized species present in a CO$_2$ plasma. By measuring changes in the structure of ALD plasma catalysts materials prepared for XRR measurement, we can characterize the robustness of the extraordinarily thin films under these conditions. Any observed changes to the properties of these films under plasma exposure can be extrapolated to changes on large scale ALD-prepared catalysts on support materials that can lead to degraded performance which could be indicated by reduced CO$_2$ conversion over time. We compared CO$_2$ plasma-exposed samples to equivalent Ar plasma-exposed samples and thermally annealed samples. These studies showed, *via* XRR measurements, that there was negligible loss of the TiO$_2$ and ZnO material at the input power (25 W), gas flow (1000 mTorr pressure CO$_2$ or Ar plasma) and duration (three hours) of experiments here. A small increase in surface roughness was observed under the plasma conditions, which was attributed to small amounts of physical film redistribution due to ion bombardment. XPS showed the formation of reduced species in the CO$_2$ plasma-exposed TiO$_2$ film, indicating the formation of oxygen vacancies under these conditions. Additionally, the plasma conditions did not cause any crystallization as was observed in the thermal annealing experiments. Overall, this work shows that ALD-derived metal oxide films can withstand CO$_2$ glow discharge plasmas for extended periods without significant mass loss or changes to the surface morphology. The conditions studied in this work are relevant to non-thermal plasma catalysis, but some reactors may operate at higher powers, resulting in higher temperatures and more rapid transformations of the interface. Further work is necessary to characterize similar film fidelity under those conditions. Regardless, these results motivate further research into more complex catalyst structures or compositions afforded by the precision of ALD synthesis.

Fig. 7 XRR spectra (from bottom to top) of as deposited (blue), thermally-annealed (magenta), Ar plasma-exposed (green), and CO$_2$ plasma-exposed (red) ALD-deposited ZnO on a polished Si wafer (substrate roughness <0.5 nm). The dashed line with each spectrum indicates the XRR spectra of the corresponding model structure. Each spectrum was offset by roughly 10^3 on the logarithmic scale in the plot to provide visual separation. The intensity for each measurement was consistent for each sample.

Data availability

The data supporting this article have been included as part of the ESI.†

Conflicts of interest

There are no conflicts to declare.

Acknowledgements

References

1 The Paris Agreement|UNFCCC, https://unfccc.int/process-and-meetings/the-paris-agreement, accessed 2024-07-19.

2 J. Rogelj, D. Shindell, K. Jiang, S. Fifita, P. Forster, V. Ginzburg, C. Handa, H. Kheshgi, S. Kobayashi, E. Kriegler, L. Mundaca, R. Séférian, M. V. Vilarino, K. Calvin, J. C. de Oliveira de Portugal Pereira, O. Edelenbosch, J. Emmerling, S. Fuss, T. Gasser, N. Gillett, C. He, E. Hertwich, L. Höglund-Isaksson, D. Huppmann, G. Luderer, A. Markandya, M. Meinshausen, D. McCollum, R. Millar, A. Popp, P. Purohit, K. Riahi, A. Ribes, H. Saunders, C. Schädel, C. Smith, P. Smith, E. Trutnevyte, Y. Xu, W. Zhou and K. Zickfeld, Mitigation Pathways Compatible with 1.5°C in the Context of Sustainable Development, in *Global Warming of 1.5 °C; Intergovernmental Panel on Climate Change*, 2018, pp. 93–174.

3 S. Rezaei, A. Liu and P. Hovington, Emerging Technologies in Post-Combustion Carbon Dioxide Capture & Removal, *Catal. Today*, 2023, **423**, 114286, DOI: 10.1016/j.cattod.2023.114286.

4 I. Adamovich, S. Agarwal, E. Ahedo, L. L. Alves, S. Baalrud, N. Babaeva, A. Bogaerts, A. Bourdon, P. J. Bruggeman, C. Canal, E. H. Choi, S. Coulombe, Z. Donkó, D. B. Graves, S. Hamaguchi, D. Hegemann, M. Hori, H.-H. Kim, G. M. W. Kroesen, M. J. Kushner, A. Laricchiuta, X. Li, T. E. Magin, S. Mededovic Thagard, V. Miller, A. B. Murphy, G. S. Oehrlein, N. Puac, R. M. Sankaran, S. Samukawa, M. Shiratani, M. Šimek, N. Tarasenko, K. Terashima, E. Thomas Jr, J. Trieschmann, S. Tsikata, M. M. Turner, I. J. van der Walt, M. C. M. van de Sanden and T. von Woedtke, The 2022 Plasma Roadmap: Low Temperature Plasma Science and Technology, *J. Phys. D:Appl. Phys.*, 2022, **55**(37), 373001, DOI: 10.1088/1361-6463/ac5e1c.

5 A. Bogaerts, E. C. Neyts, O. Guaitella and A. B. Murphy, Foundations of Plasma Catalysis for Environmental Applications, *Plasma Sources Sci. Technol.*, 2022, **31**(5), 053002, DOI: 10.1088/1361-6595/ac5f8e.

6 H. Chen, Y. Mu, S. Xu, S. Xu, C. Hardacre and X. Fan, Recent Advances in Non-Thermal Plasma (NTP) Catalysis towards C_1 Chemistry, *Chin. J. Chem. Eng.*, 2020, **28**(8), 2010–2021, DOI: 10.1016/j.cjche.2020.05.027.

7 A. George, B. Shen, M. Craven, Y. Wang, D. Kang, C. Wu and X. Tu, A Review of Non-Thermal Plasma Technology: A Novel Solution for CO_2 Conversion and Utilization, *Renewable Sustainable Energy Rev.*, 2021, **135**, 109702, DOI: 10.1016/j.rser.2020.109702.

8 G. Centi, S. Perathoner and G. Papanikolaou, *Plasma Assisted CO_2 Splitting to Carbon and Oxygen: A Concept Review Analysis J. CO2 Util.*, 2021, **54**, 101775, DOI: 10.1016/j.jcou.2021.101775.

9 I. Belov, J. Vanneste, M. Aghaee, S. Paulussen and A. Bogaerts, Synthesis of Micro- and Nanomaterials in CO_2 and CO Dielectric Barrier Discharges, *Plasma Processes Polym.*, 2017, **14**(3), 1600065, DOI: 10.1002/ppap.201600065.

10 A. H. Babikir, M. G. M. Ekanayake, O. Oloye, J. D. Riches, K. Ostrikov and A. P. O'Mullane, Plasma-Assisted CO_2 Reduction into Nanocarbon in Water Using Sonochemically Dispersed Liquid Gallium, *Adv. Funct. Mater.*, 2024, **34**(31), 2307846, DOI: 10.1002/adfm.202307846.

11 Y. Luo, X. Yue, H. Zhang, X. Liu and Z. Wu, Recent Advances in Energy Efficiency Optimization Methods for Plasma CO_2 Conversion, *Sci. Total Environ.*, 2024, **906**, 167486, DOI: 10.1016/j.scitotenv.2023.167486.

12 L. Xia, M. Wu, Y. Li, H. Guo, Y. Cheng and G. Meng, Enhancing CO_2 Conversion via Atmospheric Pressure Glow Discharge Plasma Jet Coupled with Catalysts, *Energy Fuels*, 2024, **38**(1), 565–575, DOI: 10.1021/acs.energyfuels.3c04129.

13 S. Renninger, P. Rößner, J. Stein, M. Lambarth and K. P. Birke, Towards High Efficiency CO_2 Utilization by Glow Discharge Plasma, *Processes*, 2021, **9**(11), 2063, DOI: 10.3390/pr9112063.

14 A. Bogaerts, X. Tu, J. C. Whitehead, G. Centi, L. Lefferts, O. Guaitella, F. Azzolina-Jury, H. H. Kim, A. B. Murphy, W. F. Schneider, T. Nozaki, J. C. Hicks, A. Rousseau, F. Thevenet, A. Khacef and M. Carreon, The 2020 Plasma Catalysis Roadmap, *J. Phys. D:Appl. Phys.*, 2020, **53**(44), 443001, DOI: 10.1088/1361-6463/ab9048.

15 G. Chen, R. Snyders and N. Britun, *CO_2 Conversion Using Catalyst-Free and Catalyst-Assisted Plasma-Processes: Recent Progress and Understanding J. CO2 Util.*, 2021, **49**, 101557, DOI: 10.1016/j.jcou.2021.101557.

16 D. Mei, X. Zhu, C. Wu, B. Ashford, P. T. Williams and X. Tu, Plasma-Photocatalytic Conversion of CO_2 at Low Temperatures: Understanding the Synergistic Effect of Plasma-Catalysis, *Appl. Catal., B*, 2016, **182**, 525–532, DOI: 10.1016/j.apcatb.2015.09.052.

17 D. Ray, P. Chawdhury, K. V. S. S. Bhargavi, S. Thatikonda, N. Lingaiah and Ch. Subrahmanyam, *Ni and Cu Oxide Supported γ-Al_2O_3 Packed DBD Plasma Reactor for CO_2 Activation J. CO2 Util.*, 2021, **44**, 101400, DOI: 10.1016/j.jcou.2020.101400.

18 P. Navascués, J. Cotrino, A. R. González-Elipe and A. Gómez-Ramírez, Plasma Assisted CO_2 Dissociation in Pure and Gas Mixture Streams with a Ferroelectric Packed-Bed Reactor in

Ambient Conditions, *Chem. Eng. J.*, 2022, **430**, 133066, DOI: **10.1016/j.cej.2021.133066**.

19 X. Duan, Z. Hu, Y. Li and B. Wang, Effect of Dielectric Packing Materials on the Decomposition of Carbon Dioxide Using DBD Microplasma Reactor, *AIChE J.*, 2015, **61**(3), 898–903, DOI: **10.1002/aic.14682**.

20 B. Ashford, Y. Wang, C.-K. Poh, L. Chen and X. Tu, Plasma-Catalytic Conversion of CO_2 to CO over Binary Metal Oxide Catalysts at Low Temperatures, *Appl. Catal., B*, 2020, **276**, 119110, DOI: **10.1016/j.apcatb.2020.119110**.

21 L. Wang, X. Yao, S. Jana, Y. Zhou, C. Qin, H. Shou, Y. Teng, N. Chen, L. Zhang, C. V. Singh, Z. Tan and Y. A. Wu, Interface Engineering and Oxygen Vacancy Derived from Plasma-Treated Cu_2O Synergistically Enhancing Electrocatalytic CO_2-to-C_{2+} Conversion, *J. Mater. Chem. A*, 2024, **12**, 21864–21872, DOI: **10.1039/D4TA03492A**.

22 K. V. Laer and A. Bogaerts, How Bead Size and Dielectric Constant Affect the Plasma Behaviour in a Packed Bed Plasma Reactor: A Modelling Study, *Plasma Sources Sci. Technol.*, 2017, **26**(8), 085007, DOI: **10.1088/1361-6595/aa7c59**.

23 K. Veer, S. Alphen, A. Remy, Y. Gorbanev, N. D. Geyter, R. Snyders, F. Reniers and A. Bogaerts, Spatially and Temporally Non-Uniform Plasmas: Microdischarges from the Perspective of Molecules in a Packed Bed Plasma Reactor, *J. Phys. D:Appl. Phys.*, 2021, **54**(17), 174002, DOI: **10.1088/1361-6463/abe15b**.

24 S. K. Conlin, H. Mehrabi, D. N. Parette, E. M. Nichols and R. H. Coridan, Characterizing Catalyst Function and Transformations in the Plasma Reduction of CO_2 on Atomic Layer Deposition-Synthesized Catalysts, *RSC Appl. Interfaces*, 2024, **1**, 552–563, DOI: **10.1039/D3LF00271C**.

25 C. Cardinaud, M.-C. Peignon and P.-Y. Tessier, Plasma Etching: Principles, Mechanisms, Application to Micro- and Nano-Technologies, *Appl. Surf. Sci.*, 2000, **164**(1), 72–83, DOI: **10.1016/S0169-4332(00)00328-7**.

26 F. Karouta, A Practical Approach to Reactive Ion Etching, *J. Phys. D:Appl. Phys.*, 2014, **47**(23), 233501, DOI: **10.1088/0022-3727/47/23/233501**.

27 R. Adzhri, M. K. M. Arshad, M. F. M. Fathil, U. Hashim, A. R. Ruslinda, R. M. Ayub, S. C. B. Gopinath, C. H. Voon, K. L. Foo, M. N. M. Nuzaihan, A. H. Azman and M. Zaki, Reactive Ion Etching of TiO_2 Thin Film: The Impact of Different Gaseous, in *2015 IEEE Regional Symposium on Micro and Nanoelectronics (RSM)*, 2015, pp. 1–4, DOI: **10.1109/RSM.2015.7354999**.

28 M. Huff, Recent Advances in Reactive Ion Etching and Applications of High-Aspect-Ratio Microfabrication, *Micromachines*, 2021, **12**(8), 991, DOI: **10.3390/mi12080991**.

29 K. A. M. Hiyoto, E. P. Stuckert and E. R. Fisher, Comparison of CO and CO_2 RF Plasma Treatment of SnO_2 Nanoparticles for Gas Sensing Materials, *J. Vac. Sci. Technol., A*, 2021, **39**(6), 063005, DOI: **10.1116/6.0001326**.

30 A. S. Morillo-Candas, V. Guerra and O. Guaitella, Time Evolution of the Dissociation Fraction in RF CO_2 Plasmas: Impact and Nature of Back-Reaction Mechanisms, *J. Phys.*

Chem. C, 2020, **124**(32), 17459–17475, DOI: **10.1021/acs.jpcc.0c03354**.

31 F. L. Buzzi, Y.-H. Ting and A. E. Wendt, Energy Distribution of Bombarding Ions in Plasma Etching of Dielectrics, *Plasma Sources Sci. Technol.*, 2009, **18**(2), 025009, DOI: **10.1088/0963-0252/18/2/025009**.

32 A. W. Kolfschoten, The Role of Noble Gas Ion Bombardment in Etching Reactions, *Nucl. Instrum. Methods Phys. Res., Sect. B*, 1987, **19–20**, 1001–1008, DOI: **10.1016/S0168-583X(87)80199-4**.

33 J. A. Scott, J. Bishop and M. Toth, Suppression of Surface Roughening during Ion Bombardment of Semiconductors, *Chem. Mater.*, 2022, **34**(19), 8968–8974, DOI: **10.1021/acs.chemmater.2c02391**.

34 R. Cuerno and J.-S. Kim, A Perspective on Nanoscale Pattern Formation at Surfaces by Ion-Beam Irradiation, *J. Appl. Phys.*, 2020, **128**(18), 180902, DOI: **10.1063/5.0021308**.

35 M. C. Bacariza, M. Biset-Peiro, I. Graca, J. Guilera, J. Morante, J. M. Lopes, T. Andreu and C. Henriques, *DBD Plasma-Assisted CO_2 Methanation Using Zeolite-Based Catalysts: Structure Composition-Reactivity Approach and Effect of Ce as Promoter, J. CO2 Util.*, 2018, **26**, 202–211, DOI: **10.1016/j.jcou.2018.05.013**.

36 Q. Chen, S. Meng, R. Liu, X. Zhai, X. Wang, L. Wang, H. Guo and Y. Yi, Plasma-Catalytic CO_2 Hydrogenation to Methanol over CuO-MgO/Beta Catalyst with High Selectivity, *Appl. Catal., B*, 2024, **342**, 123422, DOI: **10.1016/j.apcatb.2023.123422**.

37 Z. Liu, W. Zhou, Y. Xie, F. Liu, Z. Fang, G. Zhang and W. Jin, Highly Effective CO_2 Splitting in a Plasma-Assisted Membrane Reactor, *J. Membr. Sci.*, 2023, **685**, 121981, DOI: **10.1016/j.memsci.2023.121981**.

38 Y. Sun, J. Wu, Y. Wang, J. Li, N. Wang, J. Harding, S. Mo, L. Chen, P. Chen, M. Fu, D. Ye, J. Huang and X. Tu, Plasma-Catalytic CO_2 Hydrogenation over a Pd/ZnO Catalyst: In Situ Probing of Gas-Phase and Surface Reactions, *JACS Au*, 2022, **2**(8), 1800–1810, DOI: **10.1021/jacsau.2c00028**.

39 G. Chen, V. Georgieva, T. Godfroid, R. Snyders and M.-P. Delplancke-Ogletree, Plasma Assisted Catalytic Decomposition of CO_2, *Appl. Catal., B*, 2016, **190**, 115–124, DOI: **10.1016/j.apcatb.2016.03.009**.

40 G. Chen, N. Britun, T. Godfroid, V. Georgieva, R. Snyders and M.-P. Delplancke-Ogletree, An Overview of CO_2 Conversion in a Microwave Discharge: The Role of Plasma-Catalysis, *J. Phys. D:Appl. Phys.*, 2017, **50**(8), 084001, DOI: **10.1088/1361-6463/aa5616**.

41 P. Kaliyappan, A. Paulus, J. D'Haen, P. Samyn, Y. Uytdenhouwen, N. Hafezkhiabani, A. Bogaerts, V. Meynen, K. Elen, A. Hardy and M. K. Van Bael, *Probing the Impact of Material Properties of Core-Shell SiO_2@TiO_2 Spheres on the Plasma-Catalytic CO_2 Dissociation Using a Packed Bed DBD Plasma Reactor, J. CO2 Util.*, 2021, **46**, 101468, DOI: **10.1016/j.jcou.2021.101468**.

42 K.-R. Choi, J.-C. Woo, Y.-H. Joo, Y.-S. Chun and C.-I. Kim, Dry Etching Properties of TiO_2 Thin Films in O_2/CF_4/Ar Plasma,

Vacuum, 2013, **92**, 85–89, DOI: **10.1016/j.vacuum.2012.11.009**.

43 S. Norasetthekul, P. Y. Park, K. H. Baik, K. P. Lee, J. H. Shin, B. S. Jeong, V. Shishodia, E. S. Lambers, D. P. Norton and S. J. Pearton, Dry Etch Chemistries for TiO₂ Thin Films, *Appl. Surf. Sci.*, 2001, **185**(1), 27–33, DOI: **10.1016/S0169-4332(01)00562-1**.

44 J. Li, Y. Sun, B. Wang, H. Xiao, J. Wu, L. Chen, M. Fu and D. Ye, Effect of Plasma on Catalytic Conversion of CO₂ with Hydrogen over Pd/ZnO in a Dielectric Barrier Discharge Reactor, *J. Phys. D:Appl. Phys.*, 2019, **52**(24), 244001, DOI: **10.1088/1361-6463/ab111b**.

45 Z. Luo, S. Tian and Z. Wang, Enhanced Activity of Cu/ZnO/C Catalysts Prepared by Cold Plasma for CO₂ Hydrogenation to Methanol, *Ind. Eng. Chem. Res.*, 2020, **59**(13), 5657–5663, DOI: **10.1021/acs.iecr.9b06996**.

46 M. Q. Feliz, I. Polaert, A. Ledoux, C. Fernandez and F. Azzolina-Jury, Influence of Ionic Conductivity and Dielectric Constant of the Catalyst on DBD Plasma-Assisted CO₂ Hydrogenation into Methanol, *J. Phys. D:Appl. Phys.*, 2021, **54**(33), 334003, DOI: **10.1088/1361-6463/abfddd**.

47 J. C. Woo, G. H. Kim, J. G. Kim and C. I. Kim, Etching Characteristic of ZnO Thin Films in an Inductively Coupled Plasma, *Surf. Coat. Technol.*, 2008, **202**(22), 5705–5708, DOI: **10.1016/j.surfcoat.2008.06.077**.

48 J.-M. Lee, K.-M. Chang, K.-K. Kim, W.-K. Choi and S.-J. Park, Dry Etching of ZnO Using an Inductively Coupled Plasma, *J. Electrochem. Soc.*, 2001, **148**(1), G1, DOI: **10.1149/1.1344554**.

49 Q. Guo, N. Uesugi, T. Tanaka, M. Nishio and H. Ogawa, Reactive Ion Etching of Zinc Oxide Using Methane and Hydrogen, *Jpn. J. Appl. Phys.*, 2006, **45**(11R), 8597, DOI: **10.1143/JJAP.45.8597**.

50 P. J. Reed, H. Mehrabi, Z. G. Schichtl and R. H. Coridan, Enhanced Electrochemical Stability of TiO₂-Protected, Al-Doped ZnO Transparent Conducting Oxide Synthesized by Atomic Layer Deposition, *ACS Appl. Mater. Interfaces*, 2018, **10**(50), 43691–43698, DOI: **10.1021/acsami.8b16531**.

51 V. Miikkulainen, M. Leskela, M. Ritala and R. L. Puurunen, Crystallinity of Inorganic Films Grown by Atomic Layer Deposition: Overview and General Trends, *J. Appl. Phys.*, 2013, **113**(2), 021301, DOI: **10.1063/1.4757907**.

52 B. Abendroth, T. Moebus, S. Rentrop, R. Strohmeyer, M. Vinnichenko, T. Weling, H. Stöcker and D. C. Meyer, Atomic Layer Deposition of TiO₂ from Tetrakis(Dimethylamino)Titanium and H₂O, *Thin Solid Films*, 2013, **545**, 176–182, DOI: **10.1016/j.tsf.2013.07.076**.

53 A. L. Patterson, The Scherrer Formula for X-Ray Particle Size Determination, *Phys. Rev.*, 1939, **56**(10), 978–982, DOI: **10.1103/PhysRev.56.978**.

54 S. V. Bulyarskiy, D. A. Koiva, G. G. Gusarov, E. V. Latipov, G. A. Rudakov and V. V. Svetukhin, Crystallization of Amorphous Titanium Oxide Films upon Annealing in an Oxygen Atmosphere, *Mater. Sci. Eng., B*, 2022, **283**, 115802, DOI: **10.1016/j.mseb.2022.115802**.

55 D. A. H. Hanaor and C. C. Sorrell, Review of the Anatase to Rutile Phase Transformation, *J. Mater. Sci.*, 2011, **46**(4), 855–874, DOI: **10.1007/s10853-010-5113-0**.

56 D. H. Mei, X. B. Zhu, C. F. Wu, B. Ashford, P. T. Williams and X. Tu, Plasma-Photocatalytic Conversion of CO₂ at Low Temperatures: Understanding the Synergistic Effect of Plasma-Catalysis, *Appl. Catal., B*, 2016, **182**, 525–532, DOI: **10.1016/j.apcatb.2015.09.052**.

57 B. Bharti, S. Kumar, H.-N. Lee and R. Kumar, Formation of Oxygen Vacancies and Ti³⁺ State in TiO₂ Thin Film and Enhanced Optical Properties by Air Plasma Treatment, *Sci. Rep.*, 2016, **6**, 32355, DOI: **10.1038/srep32355**.

58 J. Moulder, W. Stickle, W. Sobol, K. D. Bomben, *Handbook of X-Ray Photoelectron Spectroscopy*, 1992.

59 R. Al-Gaashani, S. Radiman, A. R. Daud, N. Tabet and Y. Al-Douri, XPS and Optical Studies of Different Morphologies of ZnO Nanostructures Prepared by Microwave Methods, *Ceram. Int.*, 2013, **39**(3), 2283–2292, DOI: **10.1016/j.ceramint.2012.08.075**.

60 J. Zuo and A. Erbe, Optical and Electronic Properties of Native Zinc Oxide Films on Polycrystalline Zn, *Phys. Chem. Chem. Phys.*, 2010, **12**(37), 11467–11476, DOI: **10.1039/C004532B**.

61 M. Omran, T. Fabritius, E.-P. Heikkinen and G. Chen, Dielectric Properties and Carbothermic Reduction of Zinc Oxide and Zinc Ferrite by Microwave Heating, *R. Soc. Open Sci.*, 2017, **4**(9), 170710, DOI: **10.1098/rsos.170710**.

62 C. Wieckert and A. Steinfeld, Solar Thermal Reduction of ZnO Using CH₄:ZnO and C:ZnO Molar Ratios Less Than 1, *J. Sol. Energy Eng.*, 2002, **124**(1), 55–62, DOI: **10.1115/1.1434980**.

63 D. Berman and J. Krim, Impact of Oxygen and Argon Plasma Exposure on the Roughness of Gold Film Surfaces, *Thin Solid Films*, 2012, **520**(19), 6201–6206, DOI: **10.1016/j.tsf.2012.06.033**.

64 K. N. Pandiyaraj, R. R. Deshmukh, R. Mahendiran, P.-G. Su, E. Yassitepe, I. Shah, S. Perni, P. Prokopovich and M. N. Nadagouda, Influence of Operating Parameters on Surface Properties of RF Glow Discharge Oxygen Plasma Treated TiO₂/PET Film for Biomedical Application, *Mater. Sci. Eng., C*, 2014, **36**, 309–319, DOI: **10.1016/j.msec.2013.12.018**.

65 H.-K. Kim, J. W. Bae, K.-K. Kim, S.-J. Park, T.-Y. Seong and I. Adesida, Inductively-Coupled-Plasma Reactive Ion Etching of ZnO Using BCl₃-Based Plasmas and Effect of the Plasma Treatment on Ti/Au Ohmic Contacts to ZnO, *Thin Solid Films*, 2004, **447–448**, 90–94, DOI: **10.1016/j.tsf.2003.09.028**.